Journal of Fluids and Structures 35 (2012) 105–119

Contents lists available at SciVerse ScienceDirect

Journal of Fluids and Structures

journal homepage: www.elsevier.com/locate/jfs

Damping Parameters for flow-induced vibration

J. Kim Vandiver *

Massachusetts Institute of Technology Room 10–110 Cambridge, MA 02139

ARTICLE INFO

Article history:
Received 8 October 2011
Accepted 2 July 2012
Available online 10 August 2012

Keywords:
Damping
Response parameter
Mass-damping parameter
Flow-induced vibration
Scruton number

ABSTRACT

A dimensionless damping parameter, $c^* = 2c\omega/\rho U^2$, is defined for cylinders experiencing flow-induced vibration. It overcomes the limitations of "mass-damping" parameters, which first came into use in 1955. A review of the history of mass-damping parameters reveals that they have been used in three principal variations, commonly expressed as S_c, S_G and α. For spring-mounted rigid cylinders all three forms reduce to a constant times the following dimensionless group, $2c/\pi\rho D^2\omega_n$, where 'c' is the structural damping constant per unit length of cylinder and $\omega_n$is the natural frequency of the oscillator, including, when so specified, the fluid added mass. All have been used to predict $A^*_{max}=A_{max}/D$, the peak response amplitude for VIV. None are useful at organizing response at reduced velocities away from the peak in response. The proposed alternative, c^*, may be used to characterize VIV at all reduced velocities in the lock-in range. The simple product of A^* and c^* is shown to equal C_L, the lift coefficient, thus providing a simple method for compiling C_L data from free response measurements. Mass-damping parameters are not well-suited to the organization of the response of flexible cylinders in sheared flows or for cylinders equipped with strakes or fairings. c^* is well-suited for use with sheared flows or for cylinders with partial coverage of strakes or fairings. Data from three independent sources are used to illustrate the applications of c^*. It is shown that the method of modal analysis may be used to generalize the application of c^* to flexible risers. An example for a riser with partial fairing coverage is presented.

1. Introduction

The principal purpose of this paper is to introduce a damping parameter, $c^* = 2c\omega/\rho U^2$ that is useful in practical VIV response prediction of flexible structures. An example is the fatigue life prediction of a petroleum production riser in the Gulf of Mexico, exposed to the Loop Current with surface speeds in excess of three knots(1.5 m/s) and varying substantially with depth. The solution to the equations of motion of the riser requires that the power dissipated by damping be in balance with the power flowing into the riser as the result of vortex-induced lift forces. Although there are computer programs used in design that apply the principle of power balance, there is no damping parameter currently available that is able to capture the relationship between the predicted or measured riser response and the total damping, including both structural and hydrodynamic sources. c^* is shown to be able to characterize the excitation and response relationship in these more general cases.

* Tel.: +1 617 253 4366.
E-mail address: kimv@mit.edu

0889-9746/$ - see front matter © 2012 Elsevier Ltd. All rights reserved.
http://dx.doi.org/10.1016/j.jfluidstructs.2012.07.002

Nomenclature

A^*	A/D, dimensionless response amplitude
A^*_{max}	Peak A^*
b^*	dimensionless damping parameter
c^*	dimensionless damping parameter
C, c	Lumped damping constant, damping constant/length
C_a	Added mass coefficient
C_F	Total fluid force coefficient
C_L	Lift coefficient
C_P	Power coefficient
D	Cylinder diameter
f	Response frequency in Hz
f_n	Natural frequency(Hz) in vacuo
K, k	Lumped spring constant, spring constant/length
K_s, k_a	Alternative symbols for mass-damping parameters
K_d	Roughness height
M, m	Lumped mass and mass/length, both without added mass
m_a	Added mass of fluid per unit length
m^*	Mass ratio
r	Damping constant/length in some references
S_c	Scruton number
S_G	Skop-Griffin mass-damping parameter
S	Strouhal number
$y(t)$	Cross-flow response coordinate
$\overline{u}$	Turbulence intensity
$\overline{u}/U$	Turbulence level
$U^*=U/f_nD$	Reduced velocity at a fixed f_n
$V_r=U/fD$	Reduced velocity at the response frequency, f
α	Govardhan & Williamson mass -damping parameter
δ	logarithmic decrement
ζ	damping ratio
μ	Griffin's mass parameter and viscosity
ρ	density of fluid
ω	response or excitation frequency in radians / second
ω_n	natural frequency in radians/second

A secondary purpose is to understand the limitations of mass-damping parameters. In doing so the paper explores the relationship between mass-damping parameters and c^*, particularly in the context of the extensive body of research on the response of spring-supported, rigid cylinders in uniform flow. A second parameter, $b^*=2c/D\rho U$, is also found to be useful in some applications. Both c^* and b^* have properties that give them advantages over mass-damping parameters. These advantages are described in the paper.

The paper begins with a brief review of the early use of mass-damping parameters applied to flexible cantilevers in wind. It then moves onto the use of mass-damping parameters in the study of spring-mounted cylinders in uniform flow. c^* is then derived for the spring-mounted cylinder in uniform flow. The performance of c^* is illustrated with data from three different sets of experiments. The paper closes with a numerical example in which c^* is used to characterize the response of a flexible cylinder, partially covered with fairings. When exposed to a uniform flow, this cylinder has a power-in region over a fraction of its length and hydrodynamic damping over the remainder. The modal response amplitude is shown to be a smooth function of c^*.

2. A brief historical review of mass-damping from 1955 to 2006

The reader is referred to Williamson and Govardhan (2004) for a review of the principal contributors to the development of mass-damping parameters. A very brief historical summary is provided here to provide a few essential details.

2.1. Scruton, Vickery and Watkins, and Skop-Griffin

The mass-damping parameter was first introduced by Scruton in 1955 for the purpose of the characterization of the flow-induced vibration of cantilevered, flexible structures in wind. It was quickly adopted by the research community and over time came to be known as S_c, the Scruton number (Scruton, 1955, 1956, 1965, 1966); (Vickery and Watkins, 1964); (Zdravkovich, 1982):

$$S_c = 2m\delta/\rho D^2 = \pi^2 m^*\zeta. \quad (1)$$

The right-hand-side of Eq. (1) expresses the Scruton number in the currently used terms of mass ratio and damping ratio and assumes that $\delta = 2\pi\zeta$, which requires that the damping ratio be not greater than 0.3. The Scruton number was shown to work very well in collapsing maximum response amplitude data for high mass ratio cantilevers to a single curve of A^*_{max} versus S_c where $A^*=A/D$.

Griffin and colleagues attempted to expand the application of the mass-damping parameter to the prediction of the maximum response amplitude of a wide variety of flexible structures, including cables in water(Griffin et al., 1973; Griffin and Skop, 1976; Griffin and Koopman, 1977). They derived a new parameter, beginning from a wake oscillator model. After several years of attempting to perfect the model they concluded in a 1975 paper that their parameter reduced to a

constant times the Scruton number, which at the time, was referred to in the literature as k_s(Griffin et al., 1975a, 1975b). The Skop-Griffin parameter was given the symbol S_G and is defined below in terms of various old and modern symbols:

$$S_G \equiv 2\pi S^2 k_s = 2\pi S^2 \frac{2m\delta}{\rho D^2} = 2\pi^3 S^2 m^* \zeta. \tag{2}$$

The symbol S is the Strouhal number for flow past a stationary cylinder and was intended by Griffin et al. to be taken as a constant. The Griffin plots showed general trends of agreement between maximum response amplitude and S_G but there was lots of scatter to the data. This was in part due to mixing data from structures with different mode shapes and also because the dependence on Reynolds number had not yet been appreciated.

By the late 1970s critics began to point out shortcomings of mass-damping parameters as predictors of VIV response amplitude, particularly at low mass ratios (Sarpkaya, 1979). Criticism continued to accumulate, and in 1990 Zdravkovich recommended that mass-damping parameters be used only for very high mass ratio cylinders, such as structures in air (Zdravkovich, 1990). Sarpkaya gives a lengthy analysis of the deficiencies of mass-damping parameters in Sarpkaya (2004).

2.2. Two-dimensional cylinder studies by Williamson and colleagues

The goal for the use of mass-damping parameters has been to find a single parameter of the form $m^*\zeta$ which would collapse A^*_{max} experimental data onto a single smooth curve. It was not until Khalak and Williamson (1999) and Govardhan and Williamson (2006) that real progress was made in reducing the scatter in the Griffin plots. One reason for their success was the elimination of mode shape as a variable, when they simplified the problem to that of understanding the vortex-induced vibration (VIV) of two dimensional, spring-supported, rigid cylinders, in a uniform flow. They refined the familiar $m^*\zeta$ parameter to account for the influence of added mass. Their revised parameter was given the symbol α and is defined in Eq. (3):

$$\alpha = (m^* + C_a)\zeta. \tag{3}$$

This is the most general form of mass-damping parameter proposed to date. It reduces to $m^*\zeta$ when $C_a = 0.0$. When the value of C_a is changed, one must also modify the expressions for natural frequency and damping ratio as shown in Eqs. (5) and (6). Govardhan and Williamson (2006) set C_a equal to 1.0, when using α. An alternative form of α may be obtained by expressing it in terms of dimensional variables, as shown in Eq. (4):

$$\alpha = (m^* + C_a)\zeta = 2c/(\pi\rho D^2\sqrt{k/(m+m_a)}) = 2c/\rho\pi D^2\omega_n. \tag{4}$$

With precise experiments Govardhan and Williamson showed that this parameter smoothly collapsed the measured peak response, A^*_{max}, when Reynolds number was taken into account. They also showed that if Reynolds number and mass-damping were held constant, then A^*_{max} was independent of mass ratio for values from 1 to 20 (Govardhan & Williamson, 2006). The introduction of added mass in the parameter changes only the natural frequency, by a fixed amount according to the value of C_a used. For a given test arrangement and a fixed value of C_a, the natural frequency is constant, leaving the damping constant, c, as the only experimentally varied parameter, as revealed in the right-hand-side expression in Eq. (4). Because the Scruton, Griffin and Govardhan-Williamson parameters differ by only a constant factor from one another, then they all must share the same strengths and weaknesses in revealing correlations with peak response data.

The long-lasting appeal of the mass-damping parameter is due in part to an extraordinary property, as can be seen in Eq. (4) above. The parameter includes no information about the flow speed of the fluid. It is quite remarkable that without knowing the flow speed the mass-damping parameter may be used to predict the maximum response amplitude. It will be shown that this is the result of fortuitous properties of two dimensionless parameters, $U^* = U/f_nD$ and U/fD. These parameters do contain flow information, but tend to take on constant value when at the peak response amplitude, independent of the mass ratio and the level of damping, permitting the mass-damping parameter to collapse peak response data onto a smooth curve.

The spring-mounted cylinder is used in this paper as the canonical problem which may be used to compare the performance of mass-damping parameters with the proposed alternatives b^* and c^*. The analysis of the spring-mounted cylinder is presented in some detail in the next section and draws significantly on the work of Govardhan and Williamson (2006), Khalak and Williamson (1999) and Klamo et al. (2005).

3. The VIV response of spring-mounted rigid cylinders in cross-flow motion

Fig. 1 shows a simple oscillator, consisting of a uniform cylinder of structural mass M, length L, and diameter D, mounted on springs, connected to a damper and restricted to cross-flow motion. The linear dashpot constant is C. It has units of force/velocity. In this paper a lower case c is use to denote the damping constant per unit length. Hence, $c = C/L$. In a similar fashion the equivalent mass and stiffness per unit length are defined in terms of lower case letters as, $m = M/L$ and $k = K/L$. These per unit length metrics will be used henceforth. Additionally, definitions are needed for damping ratio, natural frequency and mass ratio. These are provided in Eqs. (5), (6), and (7) in which m and m_a are the structural mass and

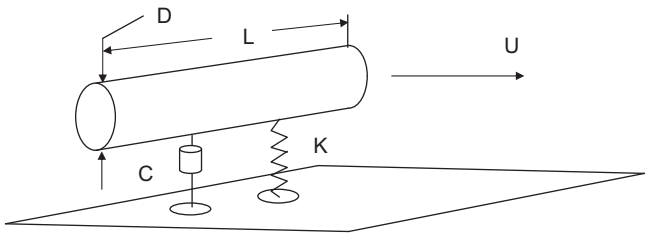

Fig. 1. Spring supported rigid cylinder with VIV in the cross-flow direction only.

fluid added mass per unit length of cylinder. ρ is the fluid density.

$$\zeta = \frac{c}{2(m+m_a)\omega_n} = \frac{c}{2\sqrt{k(m+m_a)}}, \tag{5}$$

$$\omega_n = \sqrt{\frac{k}{(m+m_a)}} \quad \text{where } m_a = C_a \rho \pi D^2/4, \tag{6}$$

$$m^* = \frac{4m}{\rho \pi D^2}. \tag{7}$$

For damping ratios less than 0.3 the logarithmic decrement is given by the simple expression $\delta = 2\pi\zeta$. For larger damping ratios the following relationships are useful: $\delta = 2\pi\zeta/\sqrt{1-\zeta^2}$, $\zeta = \delta/((2\pi)^2+\delta^2)$. For most realistic cases of VIV the damping ratio is less than 0.3 and the simpler equation will suffice. This is true for all examples used in this paper.

3.1. Dynamic equilibrium conditions for a spring-supported cylinder

The analysis of the response of a spring-mounted cylinder to VIV has been published many times including Scruton (1956). It is briefly repeated here. The equation of motion in the cross-flow direction for the cylinder shown in Fig. 1 may be written as

$$M\ddot{y} + C\dot{y} + Ky = \frac{1}{2} C_Y \rho U^2 DL \sin(\omega t + \varphi). \tag{8}$$

The principal assumption is that the cross-flow excitation is a steady-state, periodic force, which may be decomposed into a Fourier series. Because Eq. (8) is a linear, ordinary, differential equation, then by the principle of superposition the response to each Fourier component may be computed individually. The hydrodynamic force shown on the right hand side of Eq. (8) is in this case assumed to be the principal Fourier component of the cross-flow excitation. After dividing by the length, the equation may be expressed in an equivalent per unit length formulation, which will be used in the remainder of this analysis:

$$m\ddot{y} + c\dot{y} + ky = \frac{1}{2} C_Y \rho U^2 D \sin(\omega t + \varphi). \tag{9}$$

The steady state particular solution to this equation is given by $y(t) = A\sin(\omega t)$, which upon substitution into Eq. (9) leads to two Eqs. (10) and (11), shown below, in which the time dependent terms have cancelled out. Eq. (10) establishes the equilibrium relationship between the component of the fluid excitation in phase with stiffness and inertial forces in the system:

$$(k - m\omega^2)A = \frac{1}{2} C_Y \rho U^2 D \cos(\varphi). \tag{10}$$

Eq. (11) expresses the dynamic equilibrium that exists between the fluid lift force/length in phase with the cylinder velocity and $c\omega A$, the force/length required to drive the dashpot:

$$c\omega A = \frac{1}{2} C_Y \rho U^2 D \sin(\varphi). \tag{11}$$

Both Eqs. (10) and (11) are valid at any steady state excitation frequency. Eq. (10) contains all of the system information about mass, stiffness and resonance and contains no damping information. Eq. (11) has no information about the resonance properties of the system, just damping. Eq. (11) may be solved for A^* as shown in Eq. (12):

$$A^* = \frac{A}{D} = \frac{\rho U^2}{2c\omega} C_Y \sin(\varphi) = \frac{\rho U^2}{2c\omega} C_L = \frac{C_L}{c^*}. \tag{12}$$

Within the limitations of the assumption that the lift force is steady-state and periodic Eq. (12) provides the dimensionless group that governs the response amplitude. That group is called c^* in this paper and is given by:

$$c^* = \frac{2c\omega}{\rho U^2}. \tag{13}$$

In Eq. (12) the lift coefficient is defined as $C_L \equiv C_Y \sin(\varphi)$. This leads to Eq. (14), a remarkably simple expression for the lift coefficient:

$$C_L = A^* c^*. \tag{14}$$

Eq. (12) shows that A^* depends only on C_L and c^*. C_L accounts for many factors including Reynolds number. The equilibrium between lift force and damping force is accounted for by c^*. If c^* expresses the correct relationship between damping and response amplitude, it is difficult to believe that a much simpler mass-damping parameter might also work. It is shown in the next section, that under the restricted conditions which permit mass-damping parameters to successfully organize $A^*_{\max}$ data, c^* and the mass-damping parameter are simply proportional to one another, as shown in the following equation: $c^* = G(m^* + C_a)\zeta$, where G is a constant, which depends on U^* and U/fD.

c^* has been suggested previously in the literature, though represented by different symbols. In Vandiver (1993) the author derived a parameter which was equal to $c^*/2$. In Vandiver (2002) it was shown how the parameter, called c^* in this paper, could be implemented in a modal analysis prediction of the response of a flexible cylinder in sheared flow. In Vandiver and Marcollo (2003) it was shown that the parameter appears in solutions for the response of finite and infinitely long flexible cylinders in sheared flow. Although the parameter was previously derived, for the first time in this paper the applicability of the parameter is supported with experimental evidence.

3.2. Modeling cylinder response with the mass-damping parameter

Versions of Eq. (12) have been expressed by many authors, including Scruton (1956); Khalak and Williamson (1999), and Govardhan and Williamson(2006). In Govardhan and Williamson (2006) it appears as eq. 1.4 as given by $A^* = 1/(4\pi^3)(C_Y \sin\phi/(m^* + C_a)\zeta))(U^*/f^*)^2 f^*$, where $f^* = f/f_n$ and $U^* = U/f_n D$. Eq. (15) is the equivalent formulation in terms of U/fD and $U^* = U/f_n D$:

$$A^* = \frac{1}{4\pi^3}\frac{C_Y \sin\phi}{(m^* + C_a)\zeta}\left[\frac{U}{f_n D}\right]\left[\frac{U}{fD}\right]. \tag{15}$$

Equating Eqs. (12) and (15) and solving for c^* yields:

$$c^* = \left[4\pi^3 \frac{f_n D}{U}\frac{fD}{U}\right][(m^* + C_a)\zeta] = G(m^* + C_a)\zeta. \tag{16}$$

In Govardhan and Williamson (2006) the authors state that the goal of a successful mass-damping parameter is "to reasonably collapse peak-amplitude data $A^*_{\max}$ in the Griffin plot". To achieve success they go on to say "Therefore the assumption is often made that both (U^*/f^*) and (f^*) are constants under resonance conditions", giving:

$$A^*_{\max} \propto \frac{C_Y \sin\phi}{(m^* + C_a)\zeta}. \tag{17}$$

This is equivalent to saying that G in Eq. (16) is a constant, given by $G = 4\pi^3(f_n D/U)(fD/U)$. The experimental data from Govardhan and Williamson (2006) show that at $A^*_{\max}$, $U/f_n D$ and U/fD remain constant as α is varied, thus verifying that G is a constant in Eq. (16). Example data from the experiments described in Govardhan and Williamson (2006) are reproduced with permission of the authors in Figs. 2 and 3. Fig. 2 presents response A^* versus U^* for seven different values of α. The experiment was conducted on a spring-mounted vertical cylinder at a Reynolds number of 4000, measured at $A^*_{\max}$. For the seven values of α at $A^*_{\max}$ the mean and standard deviation of U^* are 5.90 and 0.16, respectively. The mean value is shown by a vertical line in the figure. At the same peak locations the mean and standard deviation of U/fD are, 5.86 and 0.16. Thus, as assumed in Eq. (17), $U/f_n D$ and U/fD are constant at $A^* = A^*_{\max}$. The factor G is therefore a constant, as given by $G = 4\pi^3(f_n D/U)(fD/U) = 3.59 \pm 0.18$.

Govardhan and Williamson then go on to show that by accounting for Reynolds number it is possible to express $A^*_{\max}$ as a function of α as shown in Eq. (18) and plotted in Fig. 3:

$$A^*_{\max} = (1 - 1.12\alpha + 0.30\alpha^2)\log(0.41 \mathrm{R_e}^{0.36}). \tag{18}$$

Fig. 3 is a plot of $A^*_{\max}$ versus α for three different values of Reynolds number, 1250, 4000, and 12000. The curve fits in the figure satisfy Eq. (18). Since it has been shown that for the data in Fig. 3, $\alpha = c^*/G$ where G is a constant, then a simple substitution for α provides an expression equivalent to Eq. (18), but formulated in terms of $c^*$and G:

$$A^*_{\max} = \left[1 - 1.12\left(\frac{c^*}{G}\right) + 0.30\left(\frac{c^*}{G}\right)^2\right]\log(0.41 \mathrm{R_e}^{0.36}).$$

Thus the effect of Reynolds number on $A^*_{\max}$ is independent of the choice of c^* or α in the equations above.

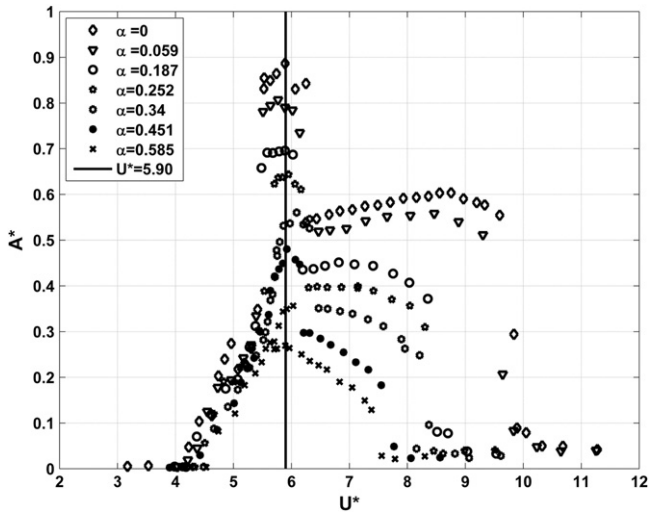

Fig. 2. A^* versus U^* for R_e=4000, m^*=10.9 and various values of damping constant. Adapted from Govardhan and Williamson (2006) Fig. 8, Vertical bar at U^*=5.90.

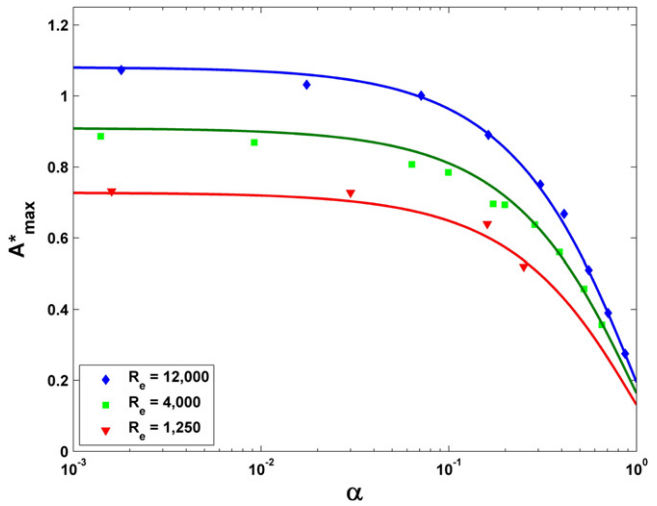

Fig. 3. A^*_{max} versus $log(\alpha)$ for R_e=1250(m^*=15.3), 4000(m^*=10.9) and 12000(m^*=10.3). Adapted from Fig. 12, Govardhan and Williamson (2006).

Eq. (18) shows that the effect of damping on response may be separated from that of Reynolds number. However, it does not provide an explicit connection between lift coefficient and Reynolds number. This is provided by Eq. (12), which says that $A^*c^*=C_L$. Because c^* is not dependent on Reynolds number, then the dependence of A^*_{max} on R_e as revealed in Eq. (18), must be embedded in a variation of C_L with R_e.

3.3. Modeling cylinder response as a function of the parameter b^*

The damping parameter b^* was first defined by Shiels et al. (2001) and then first used with experimental results by Klamo et al. (2004 , 2005). It is defined as $b^*=2c/D\rho U$ and is easily related to c^* as in shown in Eq. (19):

$$c^*=\left(\frac{\omega D}{U}\right)\left(\frac{2c}{D\rho U}\right)=\omega^* b^*, \quad where\ \omega^*=\omega D/U=2\pi f D/U. \tag{19}$$

Klamo et al. (2005) have shown that b^* collapses the plot of A^*_{max} just as well as$(m^*+C_a)\zeta$. This is shown in Fig. 4, used with permission from Klamo et al. (2005). This is peak amplitude data from spring-supported, rigid cylinder experiments. The authors showed that the effect of Reynolds number could be separated from the effect of damping. The figure shows a plot of A^*_{max} as a function of b^* for various combinations of R_e and m^*. In order for b^* to successfully collapse peak response amplitude data, c^* in Eq. (12) must be expressible as a constant times b^*. This means that the parameter ω^* must be

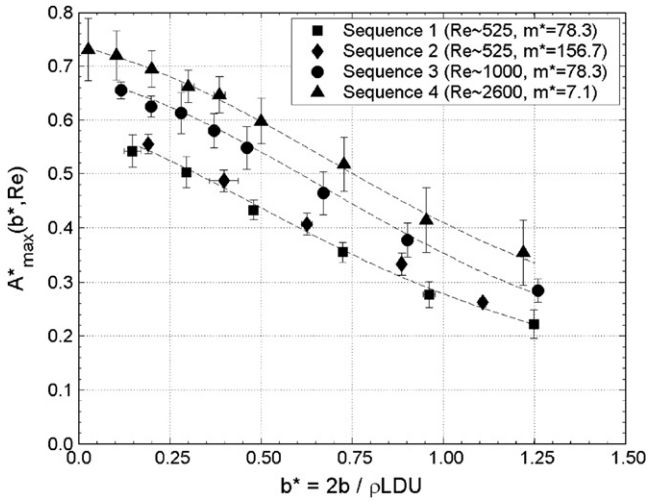

Fig. 4. A^*_{max} versus b^*, as a function of Reynolds number and mass ratio. Error bars show uncertainty in measured damping. From Fig. 2, Klamo et al.(2005).

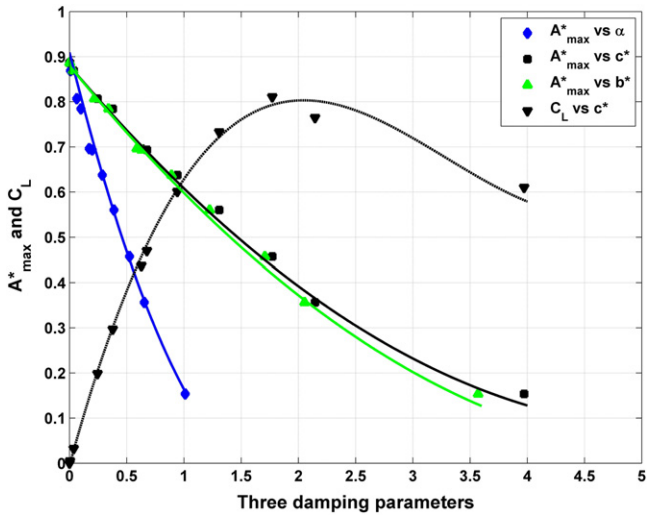

Fig. 5. A^*_{max} versus α, A^*_{max} versus c^*, A^*_{max} versus b^*, and C_L versus c^* for $Re=4000$ and $m^*=10.9$. Derived from data provided by Govardhan and Williamson (2006).

constant, which is equivalent to the requirement that U/fD be a constant, which was shown to be true in the earlier discussion of the relationship between A^*_{max} and α.

b^* may prove to be more robust than $(m^*+C_a)\zeta$ in collapsing A^*_{max} data, because using b^* requires only that U/fD be constant as b^* is varied. When using $(m^*+C_a)\zeta$, both U/fD and U/f_nD must remain constant in order for Eqs.(16) and (17) be satisfied.

3.4. The equivalence of b^*, c^* andα at A^*_{max}

It has already been shown that for the $Re=4000$ data in Figs. 2 and 3, $c^*=3.59\alpha$. For this same data the mean value of $\omega^*=1.072$. Therefore, at A^*_{max} $c^*=1.072b^*$. Fig. 5 is a plot on a linear scale of A^*_{max} versus b^*, c^* and α for the $R_e=4000$ data from Govardhan and Williamson (2006). Note that the horizontal axis serves for all three damping parameters, b^*, c^* and α. The α and b^* curves differ only by constant factors from the c^* curve. The curves for b^* and c^* are very nearly equal. This is because ω^*, the factor from Eq. (19) which relates b^* to c^*, is very nearly equal to 1.0 at A^*_{max}. Thus, when the response frequency is not available, one may roughly approximate c^* by substituting b^* or one may estimate ω^* and obtain an estimate of c^* from $c^*=\omega^*b^*$.

The use of c^* has two particular advantages over $(m^*+C_a)\zeta$ or b^*. The first is the relationship from Eq. (14), $A^*c^*=C_L$. This relationship makes it clear that the response A^*_{max} is inversely proportional to c^* and that the constant of proportionality is

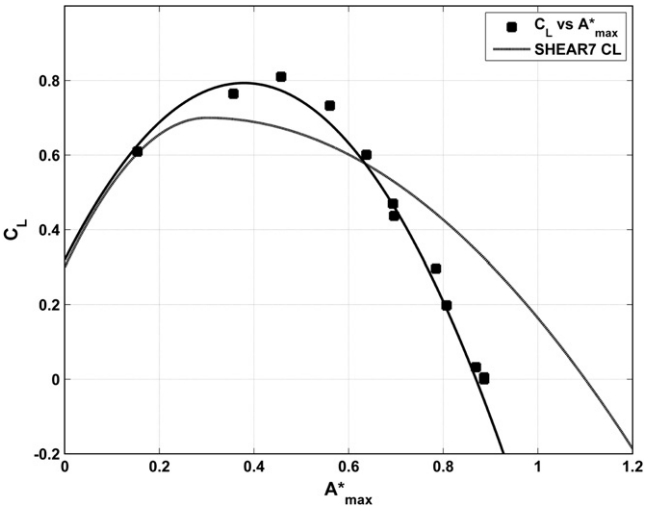

Fig. 6. C_L versus $A^*_{\max}$: (a). $Re=4000$, $m^*=10.9$ and $fD/U=0.1706$; (b). SHEAR7 Table 1 for Conservative Design.

C_L. This relationship was used to create the fourth curve in Fig. 5, a plot of C_L versus c^* at $A^*_{\max}$. The values of C_L shown in the figure are the magnitudes of the periodic dynamic lift coefficients that must have occurred in the spring-mounted cylinder experiment, so as to produce the observed peak response. These lift coefficients have been obtained, not from forced response data, but from free vibration response data. Eq. (14) is only true under dynamic response equilibrium conditions. For any given combination of damping, flow speed and natural frequency, a freely-vibrating, spring-mounted cylinder will respond at some value of A^*, corresponding to a value of C_L. In other words Eq. (14) may not be used for arbitrary combinations of A^* and reduced velocity, but only those combinations that represent dynamic equilibrium conditions.

In order to make C_L curves useful in response prediction programs, such as SHEAR7, it is necessary to tabulate C_L in terms of A^* and ω^*. Fig. 6 is an example in which the C_L data from Fig. 5 is plotted versus $A^*_{\max}$ at $\omega^*=1.072$. Also shown is a C_L curve which is implemented in SHEAR7. The SHEAR7 curve has been deduced from the analysis of a variety of sources of experimental data and has been shown to yield a conservative prediction of response of flexible cylinders at the wake-synchronized vortex shedding frequencies in uniform and sheared flows. The contributions from higher harmonics are not included. This SHEAR7 C_L curve will be used in a final example in the paper, a prediction of response for a flexible cylinder.

The second advantage is that when using c^*, no assumptions require that either U* or ω^* be constant, thus allowing use of c^* at all frequencies.

3.5. Dimensional analysis for the spring-mounted cylinder.

A list of common dimensional quantities known to be important in predicting VIV response of a spring-mounted cylinder includes: A, c, D, k, L, m, U, k_d, $\overline{u}$, ω, ρ, and μ. Of these the only variables previously not defined in this paper are k_d, $\overline{u}$, and μ. They are respectively the roughness height, the root-mean-square turbulence velocity, and the fluid viscosity. All twelve parameters are composed of at most the three fundamental units, mass, length and time, and therefore one expects to be able to find nine dimensionless groups.

The dimensional analysis proceeds by choosing three parameters to be the primary variables. In this case the three primary variables D, U and ρ were selected, and then used to obtain dimensionless groups from the nine remaining parameters. The particular selection of D, U and ρ as the primary variables guarantees that the Reynolds number is found directly. Of the nine dimensionless groups obtained by the procedure A^* was selected as the dependent parameter, which may be expressed as an unknown function of the remaining eight independent dimensionless groups, as shown in Eq. (20):

$$A^*=F\left[\mathrm{R_e}=\frac{D\rho U}{\mu},\ \frac{L}{D},\ m^*=\frac{4m}{\pi\rho D^2},\ \frac{\overline{u}}{U},\ \frac{k_d}{D},\ b^*=\frac{2c}{D\rho U},\ k^*=\frac{2k}{\rho U^2},\ \omega^*=\frac{\omega D}{U}\right]. \tag{20}$$

The first five of the eight groups are those commonly used in the VIV literature and are respectively, the Reynolds number, the length to diameter ratio, the mass ratio, turbulence intensity and the roughness. The last three are less common. b^* and k* are the dimensionless damping and stiffness used by Shiels et al.(2001) and Klamo et al.(2004, 2005, 2006). The final group is ω^* a variant of the reduced velocity: $\omega^*=(\omega D/U)=2\pi(fD/U)$. In three of the nine groups numerical constants have been added so as to make them more useful later in the paper, and to make them consistent with common usage such as in the definition of mass ratio. This does not affect their validity as independent dimensionless

groups describing the system. The reader should take note that m^* as defined here is different from that used in Klamo et al. (2005), such that $m^*_{\text{Klamo}} = \pi m^*/2$.

The theory of dimensional analysis tells us that, assuming an important physical parameter has not been omitted, the eight independent parameters found above are sufficient to completely characterize the response in terms of the dependent parameter A^*. These parameters are appropriate for all experimental conditions that might occur for the case of the spring-mounted cylinder depicted in Fig. 1.

The dimensional analysis is revealing for what does not appear: c^*, U^*, f^*, and ζ. These parameters and many others in common usage are not useful for all experimental conditions. They become useful only under restricted conditions. For example, the mass damping parameter, $(m^*+C_a)\zeta$, is useful only at A^*_{max}, which occurs only at restricted values of U^* and f^*. c^* becomes useful when the assumption is made that the response corresponds to a steady state, periodic excitation. This was the assumption made at the beginning of this paper. This assumption is valid over a wide range of conditions which allow synchronization of the wake with the cylinder motion. When that condition is met then collapsing two normally independent dimensionless parameters into one yields a useful derived parameter: $c^* = \omega^* b^*$.

4. Circumstances in which mass-damping parameters fail

4.1. The Bernitsas experimental setup

Prof. Michael Bernitsas has constructed an experimental facility for the purpose of perfecting devices, which use flow-induced vibration to extract power from flowing water, as described recently in *Mechanical Engineering* (Bernitsas, 2010). The full description of the experimental apparatus and data used here with the permission of the authors are presented in the references (Lee et al., 2011a, 2011b).

In the Bernitsas laboratory one or more single degree of freedom oscillating cylinders may be exposed to the flow in a channel. The data shown here are from a series of runs in which a single cylinder was used. The particular test conditions and system properties are given in Table 1. The experimental apparatus is mechanically equivalent to a real spring-mounted cylinder in the sense that the springs and most of the damping are not provided by actual springs and dashpots, but by virtual stiffness and damping produced by an actuator, which is feedback controlled. The feedback control system is described in Lee et al.(2011a). The system has a small amount of real mechanical damping, C_{bear}, due to sliding components and bearings. Additional damping, C_{harn}, is set in the control system, as is the virtual spring constant, K_{virtual}. Bernitsas has chosen the symbol C_{harn} to represent the damping coefficient which accounts for the power which the system is able to extract or 'harness' from the flow.

In this paper, the total damping is of interest. By defining $C_{\text{total}} = C_{\text{bear}} + C_{\text{harn}}$, the equation of motion for the equivalent mechanical system takes on exactly the same form as given previously in Eq.(8), describing a spring mounted cylinder: $M_{\text{total}}\ddot{y} + C_{\text{total}}\dot{y} + K_{\text{virtual}}y = (1/2)C_F\rho U^2 DL \sin(\omega t+\varphi)$.

All of the previous conclusions about the response of a single-degree-of-freedom cylinder exposed to a uniform flow apply to the Bernitsas system as well. Division by the length produces the equation of motion in terms of m, k and c, the mass, stiffness and damping constants per unit length: $m\ddot{y} + c\dot{y} + ky = (1/2)C_F\rho U^2 D \sin(\omega t+\varphi)$. For this system the in vacuo natural frequency is given by $f_n = [1/2\pi](\sqrt{(K_{\text{virtual}}/M_{\text{total}})}) = [1/2\pi](\sqrt{k/m})$.

This experimental technique has many new features, and the data shown here has yet to be corroborated by independent experiment. Some readers may not be convinced that a feedback control system is able to replicate the actual free vibration response of an oscillator excited by real flow. Others may be surprised by the unusually large response amplitudes measured in these experiments. Controversial or not, these data are very well suited to the purpose of this paper, which is to demonstrate that c^* is able to reveal the relationship between A^* and damping over the entire synchronization range and to do so effectively, even under conditions for which mass-damping parameters would fail. For example, these data violate the assumption that U/f_nD is a constant at A^*_{max}.

Table 1
Test parameter values corresponding to examples from Lee and Bernitsas(2011b).

M_{total}(kg)	Total system dry mass	10.94 kg
M_{added}(kg)	Added mass for $C_a = 1.0$	5.676 kg
m^*	Mass ratio(specific gravity)	1.927
D(m, inches)	Cylinder diameter	0.0889m, 3.5 inches
L(m, Feet)	Cylinder length	0.9144 m, 3.0 feet
K_{virtual}(N/m)	Virtual spring constant	400, 600, 800, 1200, 1400, 1600 and 1800 N/m
C_{bear}(N-s/m)	Fixed mechanical damping	4.4 N-s/m
C_{harn}(N-s/m)	Adjustable virtual damping	(0.0, 7.48, 14.97, 22.45, 29.94)
C_{total}(N-s/m)	Total damping	(4.4, 11.88, 19.37, 26.85, 34.34)
c_{total}(N-s/m^2)	Total damping per meter	(4.81, 12.92, 21.18, 29.37, 37.56)
U(m/s)	Variable flow velocity	Range from 0.4 to 1.4 m/s
R_e	Reynolds number	40,000 to 120,000
υ	kinematic viscosity, water	$1.1389^{*}10^{-6}$ m^2/s

4.2. Illustrating the use of c^* with data from lee and Bernitsas (2011b)

The data presented here were taken for one system mass and one mass ratio, $m^*=1.93$. All results shown in Figs. 7 to 10 used a single value of stiffness, $K=800$ N/m. Data were taken for five different values of damping coefficient, c_{total}, as summarized in Table 1. The length of the test cylinder was 3.0 feet or 0.9144 m. Table 1 also presents the damping constant per unit length of cylinder, noted as c_{total}. The damping constant per unit length is given in the legends of the figures, because it is used in the computation of c^*. For each value of damping, response was measured over a range of velocities spanning the entire VIV synchronization range.

Figs. 7 and 8 show conventional plots of A^* versus U^* and A^* versus U/fD. In these figures the five traces correspond to the five different values of c_{total}. The natural frequency used in the definition of U^* in Lee and Bernitsas (2011b) is the natural frequency in still water($C_a=1.0$), which was $f_n=1.104$ Hz for K=800 N/m. The corresponding natural frequency in air was $f_{n,\text{air}}=1.361$ Hz. For each value of c_{total} the current speed was varied in 20 to 24 discrete steps. At each speed step A^* and f were measured. To find a more complete presentation of the data, the reader is referred to Lee and Bernitsas (2011b).

The A^* values shown here are the average of the top ten peaks in the approximately steady state sample of time series data at each flow velocity. For the lowest value of damping constant the peak response, A^*_{max}, shown in Figs. 7 and 8 was in excess of 1.5 diameters. One reason for the unusually large response is that the cylinder was intentionally roughened in the region between 60 and 80 degrees, measured in both positive and negative directions back from the leading edge of the

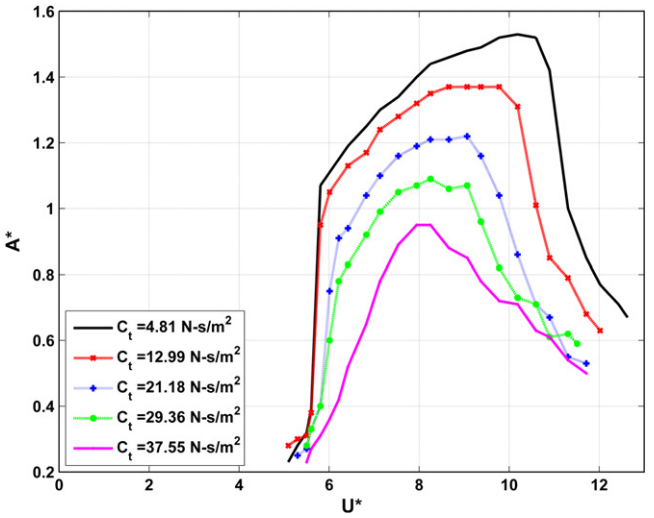

Fig. 7. A^* versus U^* for $K=800$ N/m and various values of damping constant, c_{total}; source data described in Lee and Bernitsas (2011b).

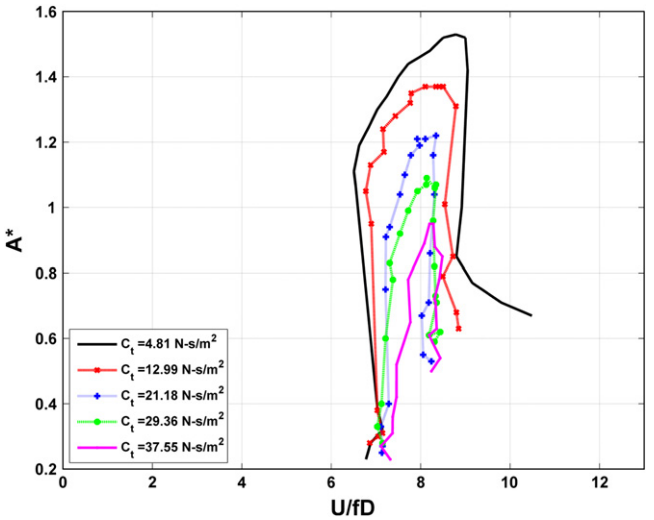

Fig. 8. A^* versus U/fD for $K=800$ N/m and various values of damping constant, c_{total}; source data described in Lee and Bernitsas (2011b).

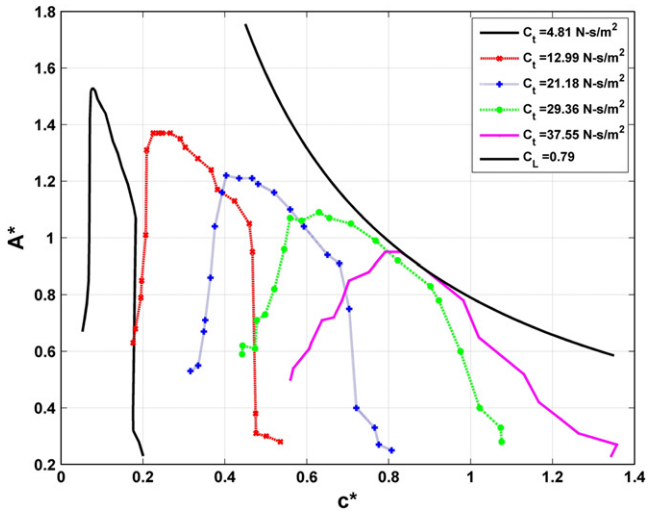

Fig. 9. A^* versus c^* for $K=800$ N/m and various values of damping constant, c_{total}; source data described in Lee and Bernitsas (2011b). The hyperbola $A^*c^* = C_{L,\max} = 0.79$ is also shown.

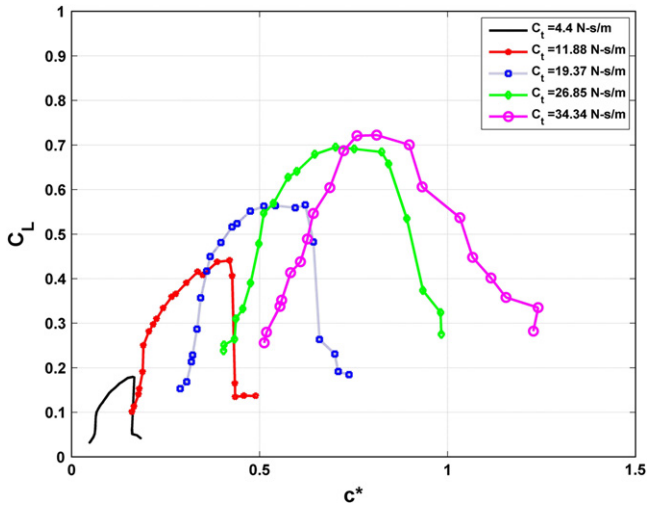

Fig. 10. C_L versus c^* for $K=800$ N/m and various values of damping constant, c_{total}; source data described in Lee and Bernitsas (2011b).

cylinder. In earlier work Bernitsas and his doctoral student *K*. Raghavan showed that roughness in this region would enhance maximum response (Bernitsas et al., 2008) and (Raghavan, 2007).

In a very recent paper (Chang and Bernitsas, 2011), it is explained that intentional use of roughness patches induces galloping of the spring-supported cylinder. In contrast to VIV, galloping is characterized by unusually large response amplitudes, lower than usual response frequencies and shedding of greater numbers of single and paired vortices per half cycle. The response shown in Figs. 7 and 8 is a mixture of ordinary VIV and galloping. The galloping tends to be associated with lower values of damping, higher values of A^* and higher values of U^*.

Examination of Fig. 7 reveals that the value of U^* at $A^*_{\max}$ does not remain constant as damping is varied. For the five different values of damping, ordered from highest to lowest damping, the values of U^* corresponding to the values of $A^*_{\max}$, were (7.94, 8.25, 9.07, 9.37, 10.19).Similarly, Fig. 8 reveals that at $A^*_{\max}$ U/fD does not remain constant as the damping is varied. However, the variation in U/fD is much less than with U^* in Fig. 7. If one were to attempt to collapse this $A^*_{\max}$ data using a mass-damping parameter, the assumption that U^* and U/fD are constant would be violated. One would have to separately account for U^* and U/fD as shown in Eq. (15).

The parameter b^* is more robust. Recall that $c^* = (\omega D/U)b^* = 2\pi(fD/U)b^*$. In order for b^* to correlate well with $A^*_{\max}$ the factor U/fD should remain constant as the damping is varied. For the data shown in Fig. 8 U/fD varies from 8.13 to 8.77 as the damping varies from largest to smallest. This is only a standard deviation of 3.3% with respect to the mean value of 8.45. Figs. 7 and 8 are plotted to the same horizontal scale, revealing visually that the variation with respect to U/fD is much less than with respect to U^*.

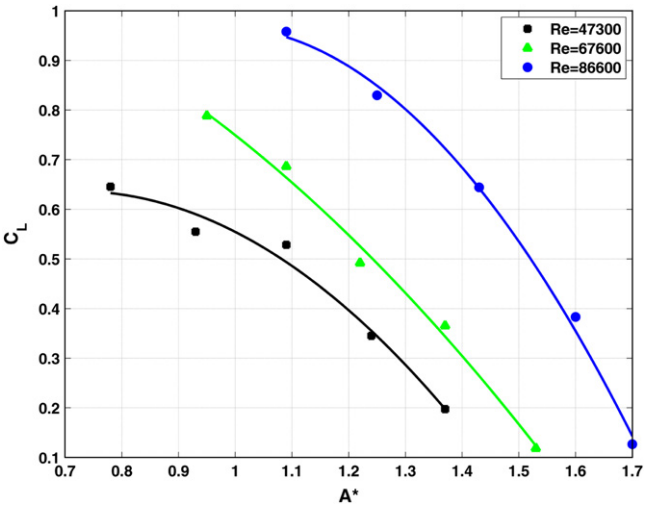

Fig. 11. C_L versus A^*_{max} for $K=400$, 800, & 1600 N/m and various values of damping constant per unit lenth, c_{total}. Average Reynolds number shown for each value of K. Source data described in Lee and Bernitsas (2011b).

By using c^*, the relationship between damping and response may be portrayed for the entire synchronization range, as shown in Fig. 9, a plot of A^* versus c^*. Each point in Fig. 9 represents the dynamic equilibrium that exists between the damping force and the fluid dynamic lift force in phase with the cross-flow velocity of the cylinder. This equilibrium is expressed by the relation $C_L=A^*c^*$, which is the equation of a hyperbola. On a plot of A^* versus c^* lines of constant C_L would appear as hyperbolas. One such hyperbola is shown in Fig. 9, corresponding to the maximum observed lift coefficient of 0.79. In Fig. 10 the variation in C_L with c^* is shown for the five different values of damping.

Fig. 11 is the final one constructed from the Lee and Bernitsas data. It is a plot of C_L versus A^*_{max} for three different values of spring constant, 400 N/m, 800 N/m and 1600 N/m. For each value of spring constant the same five values of damping constant, C_{total}, were used. Since the natural frequency varies with the square root of stiffness, this range of stiffness translates into a doubling of the in air natural frequency, as K varies from 400 to 1600 N/m. The flow velocity and therefore the Reynolds number at which peak response occurs should vary roughly in proportion to the natural frequency. In Fig. 11, for each spring constant the values of C_L versus A^*_{max} are plotted for the five different damping values. The average Reynolds number corresponding to the five data points making up each curve is given in the legend. The variation of Reynolds number ranges from 47,300 to 86,600.

Both Govardhan and Williamson (2006) and Klamo et al. (2005) have shown that A^*_{max} is dependent on Reynolds number. From Eq. (14) it is also known that $A^*c^*=C_L$. Since c^* is not a function of Reynolds number, then the Reynolds number dependence of A^* is due entirely to a Reynolds number dependence of C_L. This is revealed in Fig. 11.These results may not be directly compared to smooth cylinder data, because the cylinder used in these experiments was selectively roughened to increase response. Although the roughness has been modified, it is the same roughened cylinder for all data shown here. Therefore, one may conclude that for these experiments the lift coefficient increased with Reynolds number, which is qualitatively similar to the increase in lift coefficient that has been observed for smooth cylinders. However, much more experimental work remains to be done to properly quantify the influence of Reynolds number on the lift coefficient.

5. A role for c^* in the creation of C_L tables for practical response prediction

The design of a drilling riser for high current areas requires the prediction of the flow-induced vibration of a flexible cylinder in a sheared flow. Such predictions are the purpose of programs such as SHEAR7 (Vandiver et al., 2011), which has been in industry use since the early 1990s. Example predictions may be found in Resvanis and Vandiver (2011b). The program requires lift coefficient data tabulated as a function of A^* and ω^* or fD/U. Historically C_L tables have been compiled from data taken in forced vibration experiments. The first such data to be widely used was compiled by Ram Gopalkrishnan (1993). In his work a rigid cylinder was given an imposed, sinusoidal, cross-flow oscillation at a prescribed flow velocity and frequency. Forces were measured at the cylinder ends. From these data lift and added mass coefficient tables were created and became the basis for the earliest lift coefficient tables used in programs such as SHEAR7.

Eq. (14), $C_L=A^*c^*$, provides the means of compiling C_L versus A^* data from free vibration response measurements. An example is given in Fig. 6. It presents C_L versus A^*_{max} for two cases. One is the $R_e=4000$ data from Figs. 3 and 5. It corresponds to $U/fD=5.86$ or $\omega^*=1.072$. The second curve in that figure is one that is currently recommended to users of SHEAR7, when a conservative VIV response prediction is desired. The value of C_L is a function only of A^*. It is used by SHEAR7 to determine the C_L value for any value of fD/U that is within the lock-in bandwidth for the responding mode being analyzed. A numerical example in which this C_L curve is used by SHEAR7 is presented in the next section.

SHEAR7 has other C_L curves the user may choose from when less conservatism is required in the response estimate. In some of these curves C_L is a function of both A^* and fD/U. SHEAR7 also has C_L curves, which are intended for use in modeling risers with strakes or fairings.

6. Extending c^* to characterize the response of long flexible cylinders

It was stated in the Introduction that 'the principal goal of this paper is to establish a damping parameter that will be useful in practical VIV response prediction problems'. Although response prediction programs, such as SHEAR7 have been in use for nearly twenty years, there is no damping parameter in current use that is able to collapse predicted or measured response data for sheared flows or for risers with partial strake or fairing coverage. The following example shows how c^* may be adapted to serve this purpose.

Consider the following thought experiment. A flexible cylinder of length $L=38$ m, diameter $D=12$ mm, tension $T=1000$ N, and mass ratio $m^*=1.74$ is exposed to a uniform flow. The cylinder is protected from VIV by a fairing attached to it. With 100% fairing coverage the cylinder exhibits no VIV. Progressively the fairing is removed symmetrically from the center outwards towards the ends. The exposed portion is known as the power-in region. The length fraction of the power-in region is given by L_{in}/L, where L_{in} is the length of the central exposed region. The flow velocity is $U=1.5$ m/s. For all values of L_{in}/L greater than zero, the central region will be a source of potential VIV for several natural vibration modes. The excited modes will be those for which U^* falls within a lock-in range, such as 5.2 to 7.8, which is specified in the input data file for the program. In this example at 1.5 m/s the possible modes included in the specified reduced velocity bandwidth include modes 25 to 33.

A numerical experiment was conducted in which SHEAR7 was used to predict the response of modes 25 to 33 for power-in length fractions that vary from 10% to 100% of the total length in increments of 5%. The program computed the response of each mode individually. To do so required a lift coefficient model and a damping model, which are both built into the program. The calculation is non-linear, because both the lift coefficient model and the hydrodynamic damping depend locally on the response $A^*(z)$. The program iterates until it converges on a solution. In this example the predicted response is plotted as a function of c^* to see if there is significant correlation between c^* and the predicted response. Previously in this paper, c^* has been computed for uniform rigid, spring-mounted cylinders in uniform flow. A form of c^* is needed which is valid for flexible cylinders in sheared flow.

The lift coefficient is stored as a table in the program SHEAR7. The C_L curve used in this example is that shown in Fig. 6, as a plot of C_L versus A^*. C_L is set to be zero for regions of the riser with fairings. In the power-in zone, which is the central section without fairings, each of the modes from 25 to 33 may be excited, because they have a value of U^* that falls in the range of 5.2 to 7.8. For each mode in turn the C_L table, shown in Fig. 6, is used in an iterative algorithm, which converges to an estimate of the modal response, q_n/D, and the corresponding C_L distribution along the length of the riser. q_n is the mode participation factor for mode n.

For each excited mode the total modal damping comes from the structural sources and from hydrodynamic damping on the portion of the riser with fairings. The structural damping is specified as $\zeta = 0.003$ for this example. The hydrodynamic damping, introduced by the fairings, is computed from a formulation that is a function of the local reduced velocity and the local response amplitude as described in Vandiver (2002). The hydrodynamic damping diminishes as the power-in region grows in length. In this example the total modal damping ratio varies from 0.1 to 0.003, as L_{in}/L varies from 10 to 100%.

Vandiver (2002) describes in detail the method for the computation of modal damping coefficients, R_n, including the structural and hydrodynamic effects. The computation of the corresponding values of the modal c_n^* is described in that reference as well, although the symbol c^* was not used in that paper. The final expression for the nth mode value of c^* is presented here:

$$c_n^* = \frac{2R_n\omega}{\rho U^2 L_{in}}. \tag{21}$$

Conceptually, c_n^* may be thought of as the c^* parameter for an equivalent spring-mounted rigid cylinder of length L_{in}, and having a modal damping constant per unit length of R_n/L_{in}.

In this example SHEAR7 was used to compute the response of each mode one at a time. The modal amplitude multiplied by the corresponding mode shape yields an expression for the response of the riser due to that mode only. The non-dimensionalized modal amplitude of mode 'n' is defined as q_n/D. Fig. 12 plots q_n/D versus c_n^*: this is the magnitude of the predicted modal amplitudes (also called mode participation factors) versus the modal value of c^*.

To obtain all of the points shown in Fig. 12 the exposure fraction L_{in}/L was varied from 0.1 to 1.0 in increments of 0.05. For each value of exposed length fraction, there are approximately nine potentially responding modes, each with its own value of q_n/D and c_n^*. For each of these nine modes, the flow velocity is the same and the power-in length is the same. However, because each mode has a different natural frequency and mode shape, the solution for q_n/D and c_n^* for each mode yields slightly different results. When plotted in Fig. 12, the nine modal responses will make up a small group of points spread along a section of the curve. As the power-in length is changed, different portions of the curve, shown in Fig. 12, will be populated by points. In general the response with the smallest power-in or exposed length is at the right of Fig. 12, where c_n^* is large. The response with 100% power-in length has the highest response, as shown on the left of the curve at minimum c_n^*. This is a very simplified example, constructed to illustrate the way one would go about computing a modal

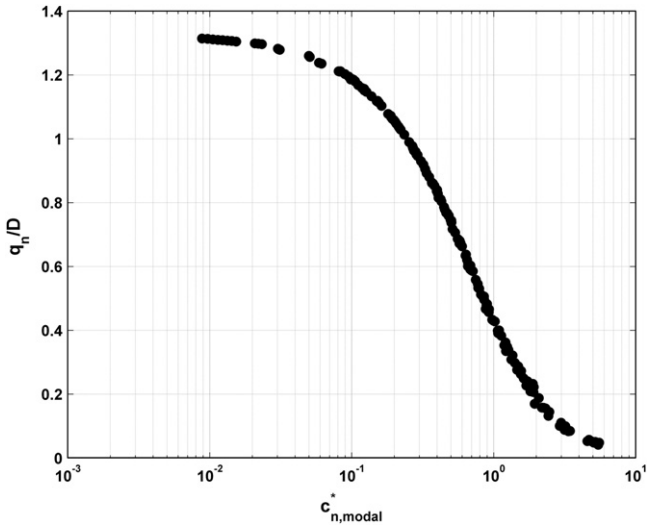

Fig. 12. Modal amplitude, q_n/D versus c^*_n from the predictions of SHEAR7 using the C_L curve from Fig. 6.

value for c^*_n, which when plotted versus q_n/D collapses the data in a way that may be easily understood and interpreted. Such an approach will work equally well for flexible cylinders in sheared flows and for structures with partial or full strake coverage.

In some SHEAR7 design computations the lift coefficient tables that are used are functions of fD/U as well as A^*. The direct consequence of this is to favor some modes in the excitation bandwidth with larger lift coefficients than others. If the lift coefficient table were made a function of both fD/U and A^*, then some of the cases shown on the curve in Fig. 12 would occur at less favorable values of fD/U, and would therefore have much lower C_L values than those used to plot Fig. 12. The curve shown in Fig. 12 would be an upper bound on the response predictions. Only those modal predictions which have ideal values of fD/U would fall near the upper bound. Many predicted modal response amplitudes would fall beneath the curve in the figure.

7. Conclusions

For spring-mounted 2-D cylinders,

i. under steady state, periodic response conditions, c^* is the damping parameter which captures the dynamic equilibrium between lift force and damping force;
ii. when mass-damping parameters are able to successfully collapse A^*_{max} data the mass-damping parameters reduce to a constant times c^*;
iii. variations in response, A^*, with Reynolds number are associated with a variation in lift coefficient with Reynolds number. The effect of c^* on A/D is separate from that of Reynolds number.
iv. c^* is valid at all frequencies in the synchronization range, not just at resonance.
v. c^* has a direct relationship to C_L via the equation $A^*c^* = C_L$. This allows C_L data to be compiled from free response experiments.
vi. when the response frequency is not known, c^* may be approximated by $b^* = 2c/D\rho U$.

c^* may be generalized to characterize the response of flexible cylinders in sheared or uniform flow, with or without strakes and fairings.

Acknowledgements

This paper draws upon many years of VIV research at MIT, which has been supported by a consortium of industrial sponsors. Current membership in the industry consortium includes AMOG Consulting, BP, Chevron, ExxonMobil, Petrobras, Shell Exploration and Production, Inc., Statoil, and Technip. The author is grateful to Prof. Charles Williamson, Dr. Raghu Govardhan, Dr. Joseph T. Klamo, Prof. Anthony Leonard, Prof. Anatol Rosko, Prof. Michael Bernitsas and Dr. Jonghun Lee for providing data which was essential to the illustrative examples in the paper. Klamo, Roshko and Leonard also provided valuable and constructive feedback on an early draft of the paper. Thanks to Christian Segura-Rivera, an MIT

undergraduate student, Themistocles Resvanis, and Zhibiao Rao, both MIT graduate students, who assisted in the preparation of figures.

References

Bernitsas, M.M., 2010. Out of the vortex. Mechanical Engineering 132, 22–27.
Bernitsas, M.M., Raghavan, K., Duchene, G., 2008. Induced Separation and Vorticity Using Roughness in VIV of Circular Cylinders at $8 \times 10^3 < Re < 1.5 \times 10^5$. In: Proceedings of International Conference of Offshore Mechanics and Arctic Engineering, Estoril, Portugal, June 15–20.
Chang, C. & Bernitsas, M., 2011. Hydrokinetic Energy Harnessing Using The Vivace Converter With Passive Turbulence Control, Proceedings of International Conference of Offshore Mechanics and Arctic Engineering, Paper No. OMAE2011-50290, Rotterdam, June 19–24.
Gopalkrishnan, R., Vortex-induced forces on oscillating bluff cylinders, Ph.D. dissertation, Massachusetts Institute of Technology, Department of Ocean Engineering, 1993.
Govardhan, R.N., Williamson, C.H.K., 2006. Defining the 'modified griffin plot' in vortex-induced vibration: revealing the effect of Reynolds number using controlled damping. Journal of Fluid Mechanics 561, 147–180.
Griffin, O.M., Koopman, G.H., 1977. The vortex-excited lift and reaction forces on resonantly vibrating cylinders. Journal of Sound and Vibration 54, 435–448.
Griffin, O.M., Skop, R.A., 1976. Vortex-induced oscillations of structures. Journal of Sound and Vibration 44, 303–305.
Griffin, O.M., Skop, R.A., Koopman, G.H., 1973. The vortex-excited resonant vibrations of circular cylinders. Journal of Sound and Vibration 31, 235–249.
Griffin, O.M., Skop, R.A., Ramberg, S.E., 1975a. Resonant, Vortex-Excited Vibrations of Structures and Cable Systems, Proceedings of the 1975 Offshore Technology Conference, Houston, Texas, May 5–8, 731–744.
Griffin, O.M., Skop, R.A., Ramberg, S.E., 1975b. Resonant. Vortex-Excited Vibrations of Structures and Cable Systems, 731–744.
Khalak, A., Williamson, C.H.K., 1999. Motions, forces and mode transitions in vortex-induced vibrations at low mass-damping. Journal of Fluids and Structures 13, 813–851.
Klamo, J.T., Leonard, A., Roshko, A., 2004. On the maximum amplitude in vortex-induced vibrations. Bulletin of the American Physical Society 49 (9), 36.
Klamo, J.T., Leonard, A., Roshko, A., 2005. On the maximum amplitude for a freely vibrating cylinder in cross-flow. Journal of Fluids and Structures 21, 429–434.
Klamo, J.T., Leonard, A., Roshko, A., 2006. The effects of damping on the amplitude and frequency response of a freely vibrating cylinder in cross-flow. Journal of Fluids and Structures 22, 845–856.
Lee, J.H., Xiros, N., Bernitsas, M.M., 2011a. Virtual damper-spring system for VIV experiments and hydrokinetic energy conversion. Ocean Engineering (in publication).
Lee, J.H., Bernitsas, M.M., 2011b. High-damping, high Reynolds VIV tests for energy harnessing using the VIVACE converter. Ocean Engineering (in publication).
Raghavan, K., 2007. Energy extraction from a steady flow using vortex induced vibration. Ph.D. University of Michigan. M.M. Bernitsas (supervisor).
Resvanis, T.L., Vandiver, J.K., 2011b, Modeling risers with partial strake coverage, Paper OMAE2011-49817, Proc. of the OMAE Conference, Rotterdam, June 2011.
Sarpkaya, T., 1979. Vortex-induced oscillations: selective review. Journal of Applied Mechanics 46.
Sarpkaya, T., 2004. A critical review of the intrinsic nature of vortex-induced vibrations. Journal of Fluids and Structures 19 (4), 389–447.
Scruton, C., 1955. Wind-excited oscillations of tall stacks. Engineer 199, 806–808.
Scruton, C., 1956. Note on the Aerodynamic Stability of Truncated Circular Cones and Tapered Stacks. National Physical Laboratory, Teddington, UK.
Scruton, C., 1965. On the Wind-Excited Oscillations of Stacks, Towers, and Masts, In: Conference Proceedings of 1963 National Physical Laboratory, Teddington, UK.
Scruton, C., 1966. Brief review of wind effects on buildings and structures. Royal Aeronautical Society Journal 70, 553–560.
Shiels, D., Leonard, A., Roshko, A., 2001. Flow-induced vibration of a circular cylinder at limiting structural parameters. Journal of Fluids and Structures 15, 3–21.
Vandiver, J.K., 1993. Dimensionless parameters important to the prediction of vortex-induced vibration of long, flexible cylinders in ocean currents. Journal of Fluids and Structures 7, 423–455.
Vandiver, J.K., (2002). A universal reduced damping parameter for prediction of vortex-induced vibration, Proc. 21st International Conference on Offshore Mechanics and Arctic Engineering, OMAE2002-28292, Oslo, Norway, June 23–28, 2002.
Vandiver, J.K., Marcollo, H.M., 2003. High mode number VIV experiments. Proceedings of the IUTAM Symposium on Integrated Modeling of Fully Coupled Fluid-Structure Interactions Using Analysis, Computations, and Experiments, 1-6 June 2003. Kluwer Academic Publishers, Dordrecht.
Vandiver, et al., 2011. SHEAR7 User's Guide. MIT.
Vickery, B.J., Watkins, R.D., 1964. Flow-induced vibrations of cylindrical structures. In: Silvester, R. (Ed.), Proceedings of the First Australasian Hydraulics and Fluid Mechanics Conference, hosted by: University of Western Australia, Crawley, Australia, 1962, Pergamon Press, New York, pp. 213–241.
Williamson, C.H.K., Govardhan, R., 2004. Vortex-induced vibrations. In: Lumley, J.L., Davis, S.H., Moin, P. (Eds.), Annual Review of Fluid Mechanics, Annual Reviews, Palo Alto, pp. 413–455.
Zdravkovich, M.M., 1982. Scruton number: a proposal. Journal of Wind Engineering and Industrial Aerodynamics 10, 263–265.
Zdravkovich, M.M., 1990. On origins of hysteretic responses of a circular cylinder induced by vortex shedding. Zeitschrift fur Flugwissenschaften und Weltraumforschung (Journal of Flight Sciences and Space Research) 14, 47–58. Springer-Verlag.